

A single-ion nonlinear mechanical oscillator

N. Akerman, S. Kotler, Y. Glickman, Y. Dallal, A. Keselman, and R. Ozeri
Physics of Complex Systems, Weizmann Institute of Science, Rehovot 76100, Israel

We study the steady state motion of a single trapped ion oscillator driven to the nonlinear regime. Damping is achieved via Doppler laser-cooling. The ion motion is found to be well described by the Duffing oscillator model with an additional nonlinear damping term. We demonstrate a unique ability of tuning both the linear as well as the nonlinear damping coefficients by controlling the cooling laser parameters. Our observations open a way for the investigation of nonlinear dynamics on the quantum-to-classical interface as well as mechanical noise squeezing in laser-cooling dynamics.

PACS numbers: 37.10.Ty 37.10.Vz

Nonlinear dynamics prevails in many dynamical systems in nature, introducing a rich behavior such as criticality, bifurcations and chaos. Nonlinear dynamics on the microscopic scale is especially interesting as it can shed light on the quantum-to-classical transition as well as provide a mean to suppress thermal and quantum noise.

All mechanical oscillators will show nonlinearity when driven far enough from equilibrium. The simplest such nonlinear oscillator is the Duffing oscillator which includes a cubic term in the restoring force [1]. Recently, such Duffing nonlinear dynamics has been extensively studied with nano-electromechanical beam resonators. The basins of attraction of a nano beam oscillator were mapped [2]. Noise squeezing and stochastic resonances were observed close to the Duffing instability [3, 4]. Noise squeezing was predicted to enable mass and force detection with precision below the standard thermal limit [5–7] and possibly below the standard quantum limit when operating close to the oscillator ground state [8].

The mechanical motion of trapped ions is highly controllable and can be efficiently laser-cooled to the quantum ground state [9]. High fidelity production of Fock, squeezed, and Schrödinger-cat states was demonstrated with a single trapped-ion [10, 11]. At the temperature range obtained with laser-cooling techniques, quadruple RF Paul traps are excellently approximated as harmonic. Nonlinearity in ion motion was observed when several ions are trapped due to their mutual Coulomb repulsion. Here nonlinearity couples between the ion-crystal normal modes, even at the single quantum level [12, 13]. Trap nonlinearities are important in the context of resonance ejection in high resolution mass spectrometry [14]. However, in these experiments ions are typically not laser-cooled and furthermore the effect of Coulomb nonlinearities in the large ion cloud is intertwined with that of the trap. Recently, amplification saturation of a single-ion “phonon laser”, resulting from optical forces that are nonlinear in the ions velocity, was demonstrated [15].

Here, we study the nonlinear mechanical response of a single laser-cooled $^{88}\text{Sr}^+$ ion, in a linear RF-Paul trap. The nonlinearity originates from the higher than quadrupolar order terms in the trapping potential. We

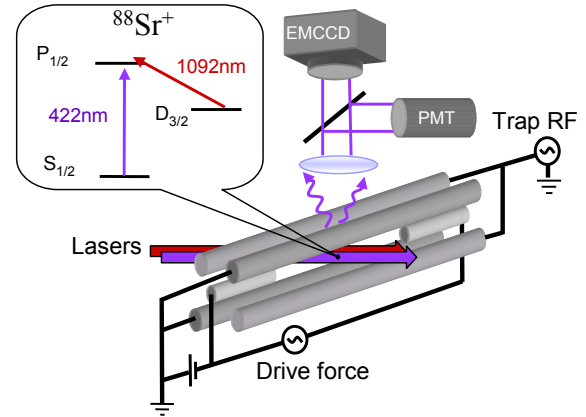


FIG. 1: Schematic diagram of the experimental set-up and the relevant energy levels of $^{88}\text{Sr}^+$ ion. The positively biased trap end-caps produce a static trapping potential in the axial direction with a small anharmonicity. The ion oscillator is driven to the nonlinear regime by a small oscillating voltage on one of the trap end-caps. Violet and infra-red laser beams provide laser cooling and optical pumping. Scattered violet photons are collected by an imaging system and directed either to an EMCCD camera or to a PMT.

find that the ion steady state response is well described by the Duffing model with an additional nonlinear damping term [16]. Unlike other realizations of nonlinear mechanical oscillators, both the linear and the nonlinear damping components can be precisely controlled.

Our trap has the canonical linear four rods and two end-caps configuration shown in Fig. 1. The distance of the ion to the end-caps and rod-electrodes is 0.65 mm and 0.27 mm respectively. Here we examine only the motion along the axial direction of the trap. In this direction, trapping is dominated by the static electric potential due to a positive constant voltage on the trap end-caps. This potential is well approximated to be harmonic with $\omega_0/2\pi = 438$ KHz. However, as the trap end-caps do not satisfy the pure electric quadrupole boundary condition, a small octupolar contribution to the electric field results a positive cubic term in the restoring force and an energy level difference of $\hbar\omega_0 + \hbar\Delta_{nl}n$ where n is the harmonic oscillator quantum number and $\Delta_{nl}/2\pi = 0.8$ mHz is the

nonlinear dispersion. This nonlinearity becomes increasingly important with growing oscillation amplitude. The ion is driven to the nonlinear regime by adding a small oscillating voltage to one of the trap end-caps. The ion is Doppler-cooled by scattering photons from a single laser beam, slightly red-detuned from the $S_{1/2} \rightarrow P_{1/2}$ transition at 422 nm. To prevent population accumulation in the $D_{3/2}$ meta-stable level we repump the ion on the $D_{3/2} \rightarrow P_{1/2}$ transition at 1092 nm.

We measure the steady-state oscillation amplitude of the ion as we slowly scan the drive frequency, ω , across the harmonic resonance, ω_0 . The scan is from lower to higher frequencies (positive sweep) or vice versa (negative sweep). Photons scattered during the cooling process are collected by an imaging system (N.A. = 0.31), and are either directed towards an Electron-Multiplying CCD (EMCCD) camera or a Photo Multiplier Tube (PMT).

We measure the amplitude of motion by taking time-averaged images of the ion as shown in Fig.2(a). The image is then integrated along the direction perpendicular to motion to produce a single curve. Every column in Fig. 2(b) corresponds to a curve produced this way, for a positive frequency sweep. As seen, the oscillation amplitude increases as the drive frequency approaches ω_0 , continues to increase passed ω_0 , until at a given critical drive frequency, ω_m , abruptly collapses to a significantly lower value. We extract the ion oscillation amplitude by fitting the curve to the expected time-averaged position distribution. The blue and red lines in Fig. 3 are the measured amplitudes for positive and negative sweeps respectively. Different curves correspond to different drive amplitudes. The asymmetry and hysteresis as well as the abrupt amplitude changes at specific critical drive frequencies are a clear deviation from the driven harmonic oscillator response. As expected from a positive nonlinearity, the oscillator self-frequency is “pulled” to higher values at higher oscillation amplitudes.

In order to measure the phase difference between the ion-oscillator and the driving force, we time-stamp each photon measured by the PMT within a single drive period to allocate it with a corresponding drive phase. The instantaneous photon scattering rate from the cooling laser beam is determined by the ions’ instantaneous velocity through its associated Doppler shift [17]. A histogram of the measured photon phases is shown in Fig.2(c). A clear sinusoidal oscillation of the photon scattering rate yields the ion-oscillator phase. The columns in Fig.2(d) are photon phase histograms for a positive drive frequency sweep. As seen, at the critical frequency, ω_m , a phase jump of 1.2 radians in the oscillator motion accompanies the sudden change in oscillation amplitude.

Our observations are well accounted for by the Duffing oscillator model. The Duffing equation of motion is,

$$\ddot{x} + 2\mu\dot{x} + \omega_0^2x + \alpha x^3 = k \cos(\omega t). \quad (1)$$

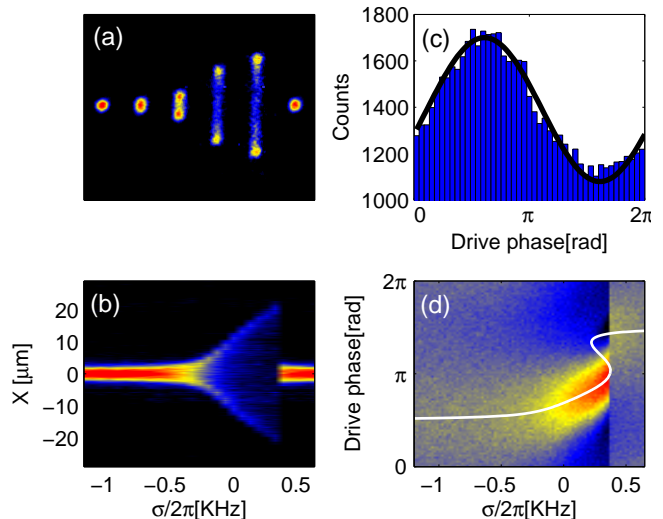


FIG. 2: Driven ion-oscillator amplitude and phase. (a) Time-averaged ion images taken at various drive frequencies. (b) Columns are time-averaged images, integrated along the direction perpendicular to ion-motion, during a positive frequency scan. (c) A histogram of the number of photons detected at different driving force phases. (d) Columns are photon phase histograms taken during a positive frequency scan. The solid line is the theoretical phase given by Eq.3 shifted by a constant to match the peak in the histograms.

Here x is the displacement of the ion from its equilibrium position, α is the an-harmonic coefficient, μ is the linear damping coefficient and k is the drive amplitude. The recoil noise inherent to the spontaneous photon scattering process, which would appear as a Langevin force term, is neglected. An approximate solution to Eq.1 can be obtained by the multiple scale method [1]. Here the solution has the form $x(t) = a(t) \cos(\omega t - \phi)$, where $a(t)$ is a slowly-varying oscillation amplitude and ϕ is the oscillator phase. The steady-state solution for a solves,

$$\sigma = \frac{3\alpha}{8\omega_0} a^2 \pm \sqrt{\frac{k^2}{4\omega_0^2 a^2} - \mu^2}, \quad (2)$$

where $\sigma = \omega - \omega_0$ is the drive detuning. The steady-state solution for a , at a fixed k , vs. drive frequency is shown by the black line in the inset of Fig.3. Above a critical amplitude a_c , a trifurcates into three solutions. One solution with small and one with large amplitude, are stable, while the third, intermediate amplitude solution, is unstable and is positioned on the state-space separatrix. This bistability persists until the high amplitude solution reaches a maximal value, a_m , at which the drive force is overwhelmed by damping and the oscillator is forced into a single stable solution. Positive and negative frequency scans carry the oscillator into the bistability region along different stable attractors leading to the observed hysteresis as illustrated by the arrows in the inset. To compare with our data we independently measure all the pa-

parameters in Eq.1. The driving force amplitude, k , is measured by observing ion displacement vs. end-cap voltage, ω_0 is measured via ion response in the linear regime. A value of $\alpha/4\pi^2 = 1.24 \pm 0.03 \cdot 10^{18} \text{ Hz}^2/\text{m}^2$ is measured using the observed dependence of a_m on $\sigma_m = \omega_m - \omega_0$, the instability detuning, $a_m = \sqrt{8\omega_0\sigma_m/3\alpha}$. A value of $\mu/2\pi = 39.2 \pm 0.3 \text{ Hz}$, which result in a quality factor $Q = 5590$, is evaluated using the variation of a_m with the drive amplitude, $a_m = k/(2\mu\omega_0)$. The blue and red circles in the inset are the measured amplitudes, for positive and negative scans respectively, showing good agreement with the theoretical curve.

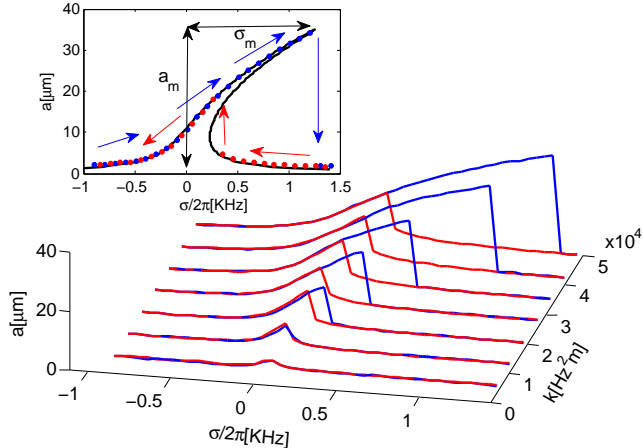


FIG. 3: Measured oscillator amplitude vs. drive frequency for various driving force amplitudes and both positive (blue) and negative (red) scans. The inset shows the Duffing model calculation (black solid line) and our measured amplitudes (blue circles - positive scan; red circles - negative scan)

The Duffing oscillator steady state phase is given by,

$$\tan(\phi) = \frac{8\mu\omega_0}{3\alpha a^2 - \omega_0\sigma}. \quad (3)$$

The white solid line in Fig.2(d) shows the theoretical phase curve vs. drive frequency for our experimental parameters, showing good agreement with our data.

Linear damping is a very good approximation for most mechanical oscillators, as typically dissipation originates from coupling of the oscillator to an ohmic bath. Recently, the contribution of non-linear damping to the motion of a nano beam resonator was studied [19]. In our experiment damping results from the change in radiation pressure vs. ion velocity. When the laser frequency is tuned below the cooling transition, the leading contribution is indeed linear in the ions' velocity. However, as the oscillation amplitude increases or the cooling-laser detuning reduced, the effect of damping force terms that are nonlinear in the ions' velocity increases [17].

To account for nonlinear damping, Eq.1 is modified to include a term which is cubic in the oscillator velocity,

$$\ddot{x} + 2\mu\dot{x} + \gamma\dot{x}^3 + \omega_0^2x + \alpha x^3 = k \cos(\omega t). \quad (4)$$

Here γ is the cubic damping coefficient. The steady-state amplitude is now a solution of [18, 19],

$$\frac{9}{16}(\alpha^2 + \gamma^2\omega_0^6)a^6 + 3\omega_0(\mu\gamma\omega_0^3 - \sigma\alpha)a^4 + 4\omega_0^2(\sigma^2 + \mu^2)a^2 - k^2 = 0. \quad (5)$$

When $\gamma > 0$, nonlinear damping acts to effectively increase dissipation for larger oscillation amplitudes. Unlike the linear damping case, a_m does not increase linearly with k but is rather limited by the growing dissipation. We find μ and γ by a maximum likelihood fit of the measured a_m vs. k curve to the solution of Eq. 5. It is instructive to look at the responsivity, $\chi = 2\mu\omega_0 a/k$, in order to distinguish linear from nonlinear damping [18]. In Fig.4 we plot the measured χ for positive scans and various drive amplitudes, k , for two different cooling-laser detuning values, δ . In Fig.4(a) $\delta/2\pi = -420 \text{ MHz}$, $\gamma = 0$ and the maximal responsivity is seen to be independent of k . In Fig.4(b) $\delta/2\pi = -160 \text{ MHz}$, $\omega_0^2\gamma/2\pi = 0.09 \pm 0.002 \mu\text{m}^{-2}\text{Hz}$ and the maximal responsivity decreases as k increases. The linear dissipation term, μ , is similar in both cases. The solid lines are the solutions of Eq.5 showing good agreement with the data.

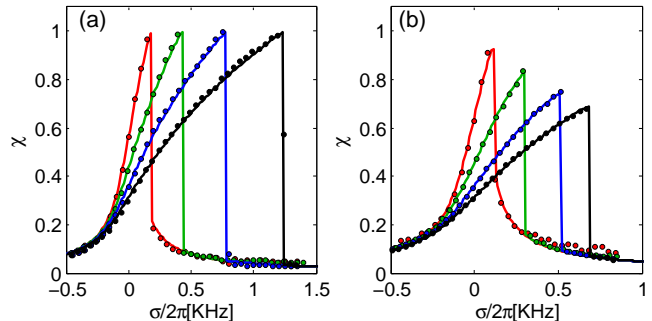


FIG. 4: Calculated and measured responsivity, $\chi = 2\mu\omega_0 a/k$, for positive drive scans. Different curves correspond to different drive amplitudes. Due to small drifts in ω_0 ($<100\text{Hz}$) each curve was separately shifted on the frequency axis to fit the theoretical curve. (a) Linear damping, the cooling laser detuning $\delta/2\pi = -420 \text{ MHz}$ and $\gamma = 0$. The maximal responsivity is independent of drive amplitude k . (b) Nonlinear damping, $\delta/2\pi = -160 \text{ MHz}$ and $\omega_0^2\gamma/2\pi = 0.09 \mu\text{m}^{-2}\text{Hz}$. The maximal responsivity decreases as k increases.

We next repeat the measurement of μ and γ for various cooling-laser detunings at a fixed repump-laser frequency and lasers intensities. The measured μ and γ vs. δ are shown in figures 5(a) and 5(b) respectively. To compare with the theoretically predicted values we write the cooling-laser scattering force,

$$F_s(\dot{x}) = \hbar k_c \Gamma \rho_p (\delta_c + k_c \dot{x}, \delta_r + k_r \dot{x}), \quad (6)$$

where $k_{c/r}$ and $\delta_{c/r}$ are the wave-vectors and detunings of the cooling and repump lasers respectively, $\Gamma = 2\pi \times 21 \text{ MHz}$ is the spectral linewidth of the $P_{1/2}$ level and

ρ_p is the $P_{1/2}$ population. The damping coefficients are therefore given by the appropriate derivatives,

$$\mu = \frac{1}{2m} \frac{dF_s}{d\dot{x}} ; \quad \gamma = \frac{1}{6m} \frac{d^3F_s}{d\dot{x}^3}. \quad (7)$$

Here m is the ion mass. We calculate ρ_P by numerically solving the eight coupled Bloch equations, corresponding to the population in all states in the $S_{1/2}$, $P_{1/2}$ and $D_{3/2}$ levels coupled by the cooling and repump lasers. The cubic damping coefficient is highly sensitive to different laser parameters due to the presence of dark resonances. The solid lines in figures 5(a) and 5(b) are the calculated μ and γ showing good agreement with our measured values. The two lasers intensities and the repump-laser detuning were used as fit parameters, yielding values that agree within 20% with their measured value.

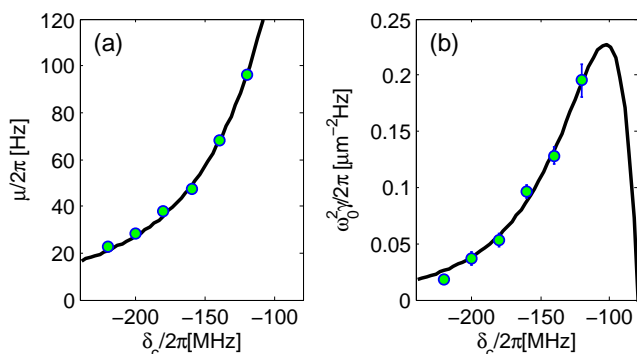


FIG. 5: (a) Linear and (b) cubic damping coefficients for various cooling-beam detunings. Filled circles are measured values and solid lines are calculated using equations 6 and 7.

An additional nonlinear damping term, proportional to $x^2\dot{x}$, results from the laser beam finite size (100 μm FWHM) and has an identical effect to that of γ on the steady-state motion [16, 18]. This term was calculated to be small relative to γ [20] and was taken into account in Fig.5.

In conclusion, we have driven a single-ion oscillator to the nonlinear regime. The ion steady-state motion, showing a bifurcation into two stable attractors and hysteresis, is well described by the Duffing oscillator model with an additional nonlinear damping term. Unlike previously studied nonlinear mechanical oscillators, here both the linear and nonlinear parts of dissipation can be tuned with the cooling laser parameters.

The study of the nonlinear motion of trapped laser-cooled ions opens several exciting research avenues. Since trapped atomic-ions can be cooled to the quantum ground state, they are an excellent platform to study nonlinear behavior in the quantum regime. As shown in [21], unlike the simple harmonic oscillator, a Duffing oscillator will demonstrate a clear quantum-to-classical transition even when classically driven. Moreover, as the

ion-spin can be entangled with its motion, it will be possible to form a coherent superposition of the two attractors states of motion. Laser-cooling of a nonlinear driven ion-oscillator has several interesting aspects that can be further explored. Since the Doppler shifts associated with the oscillation amplitudes in the nonlinear regime are significant compared with the cooling transition linewidth, the laser-cooling force is largely nonlinear in the oscillator velocity. Furthermore, the thermal state generated by laser-cooling is the result of balance between the damping force and the inherent heating due to the recoil noise from spontaneous photon scattering. Close to the Duffing instability, the ion-oscillator response to noise is quadrature dependent. One noise quadrature is largely enhanced whereas the other quadrature is suppressed [3]. Laser-cooling in this case is likely to produce squeezed states of motion.

This work was partially supported by the ISF Morasha program and the Minerva foundation.

-
- [1] A. H. Nayfeh and D. T. Mook, *Nonlinear Oscillations*, ser. Wiley Classics Library. New York: Wiley, 1995.
 - [2] I. Kozinsky *et al.*, Phys. Rev. Lett. **99**, 207201 (2007).
 - [3] R. Almog, S. Zaitsev, O. Shtempluck, and E. Buks, Phys. Rev. Lett. **98**, 078103 (2007).
 - [4] R. L. Badzey and P. Mohanty, Nature **437**, 995 (2005).
 - [5] B. Yurke, D. S. Greywall, A. N. Pargellis, and P. A. Busch, Phys. Rev. A **51**, 4211 (1995).
 - [6] E. Buks and B. Yurke, Phys. Rev. E **74**, 046619 (2006).
 - [7] J. S. Aldridge and A. N. Cleland, Phys. Rev. Lett. **94**, 156403 (2005).
 - [8] E. Babourina-Brooks, A. Doherty, and G. J. Milburn, New. J. Phys. **10**, 105020 (2008).
 - [9] D. Leibfried, R. Blatt, C. Monroe, and D. J. Wineland, Rev. Mod. Phys. **75**, 281 (2003).
 - [10] D. M. Meekhof *et al.*, Phys. Rev. Lett. **76**, 1796 (1996).
 - [11] C. Monroe, D. M. Meekhof, B. E. King, D. J. Wineland, Science **272**, 1131 (1996).
 - [12] C. Marquet, F. Schmidt-Kaler, D. F. V. James, Appl. Phys. B **76**, 199 (2003).
 - [13] C. F. Roos *et al.*, Phys. Rev. A **77**, 040302(R) (2008).
 - [14] A. A. Makarov, Anal. Chem. **68**, 4257 (1996)
 - [15] K. Vahala *et al.*, Nature Physics **5**, 682 (2009).
 - [16] B. Ravindra and A. K. Mallik Phys. Rev. E **49**, 4950 (1994)
 - [17] As the life-time of the $P_{1/2}$ level (8 ns) is much shorter than the oscillation period (228 ns), the photon scattering rate instantaneously adjusts as the ions' velocity varies.
 - [18] R. Lifshitz and M. C. Cross, Review of Nonlinear Dynamics and Complexity **1**, 1 (2008)
 - [19] S. Zaitsev, O. Shtempluck, E. Buks, and O. Gottlieb arXiv:cond-mat/053130v1 (2005).
 - [20] The ratio between the two terms depends on the cooling laser detuning and is always below 0.2.
 - [21] I. Katz, A. Retzker, R. Straub, and R. Lifshitz, Phys. Rev. Lett. **99**, 040404 (2007).